Arch. Metall. Mater. **69** (2024), 2, 471-474

DOI: https://doi.org/10.24425/amm.2024.149769

JIN WOO KIM[1], DONG WAN LEE[1], SU GWAN LEE[1], DINH VAN CONG[1], JIN CHUN KIM[1*]

MICROSTRUCTURE ANALYSIS AND POWDER BED FUSION OF INCONEL 738 POWDER MATERIALS MIXED WITH NANO-SIZED CERAMIC POWDERS

Powder materials strengthened by oxide dispersion are generally made by *in-situ* method; direct oxide dispersing in matrix powders during atomization. There is also *ex-situ* method; oxides dispersing by mixing with matrix powders. In this study powder mixtures (Inconel 738 matrix powder + SiO_2 powder + Al_2O_3 powder) were mechanically manufactured by *ex-situ* process, a low-energy ball milling method. Then, specimens of the as-mill powders were manufactured by laser powder bed fusion (L-PBF) method and spark plasma sintering (SPS) process. The microstructures of each prepared specimen were compared according to process variables. SEM, EDS, XRD, and Electron Backscatter Diffraction (EBSD) analyses were applied in this study.

Keywords: Additive Manufacturing; LPBF; Inconel738 Powder; Microstructure analysis

1. Introduction

Oxide dispersion strengthened (ODS) superalloys with high-temperature resistance and mechanical properties are used in defense, power industries and aerospace industries [1,2]. The strengthening is normally achieved by fine oxide (Y_2O_3, ThO_2, etc.) or carbide particles in a metal matrix [3]. In order to disperse the fine oxide or carbide powder in the metal matrix, two methods of the *in-situ* process and the *ex-situ* process are generally used [4].

In *in-situ* method, the oxides or carbides are included or dispersed directly in the powder matrix during the powder atomization process [5]. On the other hand, in *ex-situ* method, the oxides or carbides was mixed or mechanically alloyed with the matrix powder by ball milling or high energy ball milling process [6,7]. However, in both processes, the traditional sintering powder metallurgy or hot isostatic process (HIP) has been applied to obtain a final sintered part [8,9]. These P/M and HIP have limitations to make the complex shaped products. So recently, a new process called 3D printing, additive manufacturing, has developed extensively.

In this research, we used a commercial Inconel 738 powder to compare with MA6000, a well-known ODS Ni superalloy [10]. In this powder, ceramic oxide powders were mixed by an *ex-situ* method using a low-energy simple ball mill process. The final samples were prepared by a laser powder bed fusion (L-PBF) process using the *ex-situ* mixed powders. In addition, in order to compare the differences in the microstructure and densification behaviors, the prepared powder was conducted by the spark plasma sintering (SPS) process [11]. The microstructures of each prepared specimen were compared according to process variables.

2. Experimental

Powder mixtures were prepared by a low-energy ball-milling method using Inconel 738 after mixing nano-sized SiO_2 and Al_2O_3 powders. Powder characteristics were analyzed before and after mixing. The particle size distribution of the powder was observed using a laser powder size analyzer. The particles' shape was analyzed using SEM. EDS analysis was performed to identify the elemental composition of the mixed powder.

The additive manufacturing, 3D printing, was done by Metal3D-MetalSys120D (Korea Rep.), L-PBF machine. The manufacturing conditions were the following: layer 30 μm, spot 70 μm, hatch interval 200 μm, pattern: chess board, laser power 150-160 W, and laser speed 860-1000 mm/s.

To compare with the L-PBF method, the specimens sintered using SPS equipment were prepared by SPS-515S (Sumitomo Coal Mining). The SPS pressure was 45 MPa (3.5 kN) and the sintering temperature was 1000°C.

[1] UNIVERSITY OF ULSAN, SCHOOL OF MATERIALS SCIENCE & ENGINEERING, ULSAN, REPUBLIC OF KOREA

* Corresponding author: jckimpml@ulsan.ac.kr

The scanning electron microscope (JEOL-IT200, Japan) was applied to study the microstructure of samples. The samples were polished with sandpaper from #220 to #2000 and then they finely polished with 1 μm alumina suspensions. The etching treatment was performed with an HCl-CH_3COOH-HNO_3 acid solution. EBSD analyses for the samples were performed to observe the crystal orientation with the process.

3. Results and discussion

SEM image and XRD result of the pure Inconel 738 powder is shown in Fig. 1(a). The powder has spherical shape with a smooth surface. SEM image, XRD pattern, and EDS point of the mixed powders are shown on Fig. 1(b) and (c). Due to the powder was mixed by a low-energy ball milling method, the morphology of the mixed powder is observed to be spherical. The nano sized SiO_2 and Al_2O_3 particles were well coated on the surface of the Inconel 738 powders as shown in EDS result. As XRD result of the mixed powder, it could be seen that the peak of the nano ceramic oxide was not detected. This is due to the ratio of the nanoparticles is very small at 1% and the size of the nanoparticles is very small. The results of EDS analysis on particles on the surface of the mixed powder are shown in TABLE 1.

TABLE 1

EDS Analysis Results of the mixed powder (spc_001 point in Fig. 1(c))

Elements	Mass%	Atom%
O	58.66 ± 1.48	71.28 ± 1.80
Al	3.85 ± 0.54	2.77 ± 0.39
Si	37.49 ± 1.63	25.95 ± 1.13
Total	100.00	100.00

On the other hand, we found that the prepared ball milled mixed- powder would be not suitable for the 3D printing. The flow rate of the mixed powder decreased to 27.47 s/50 g compared to 17.39 s/50 g of pure Inconel 738 powder. However, the Hausner ratios of each powder were 1.11 and 1.15, respectively, so there was no problem in 3D printing. The results of the characteristic analysis of the powder are shown in TABLE 2.

TABLE 2

Analysis results of Characteristics of Inconel 738 Powder and Mixed Powder

	Flowability (s/50g)	Apparent Density (g/cm^3)	Tap Density (g/cm^3)	Hausner Ratio
Pure Inconel 738 Powder	17.39	4.02	4.46	1.11
Mixed Inconel 738 Powder	27.47	3.86	4.44	1.15

Fig. 2 is shown the side view of the SEM, TEM and EDS mapping images of the specimen after L-PBF. Both Inconel 738 specimen (Fig. 2(a) and mixed powder specimen (Fig. 2(b) had fine dendrite structure and needle-shaped microstructure grown in the Z direction [12,13]. Elements Ni and Ti presented in Inconel 738 were detected by EDS (Fig. 2(a)). Mapping analysis of the mixed powder specimens also shows the Al and Si elements (Fig. 2(b) by adding nano-ceramic powder. It means the nano-ceramic powders were well dispersed in the Inconel 738 matrix. Fig. 2(c) shows the results of TEM and EDS mapping analysis of the Mixed Inconel 738 PBF specimen. The size of nano oxide particles from the TEM image is about 34-58 nm.

Fig. 3 shows the results of EBSD analysis of L-PBF and SPS samples. IPF map, and phase map were also included in the

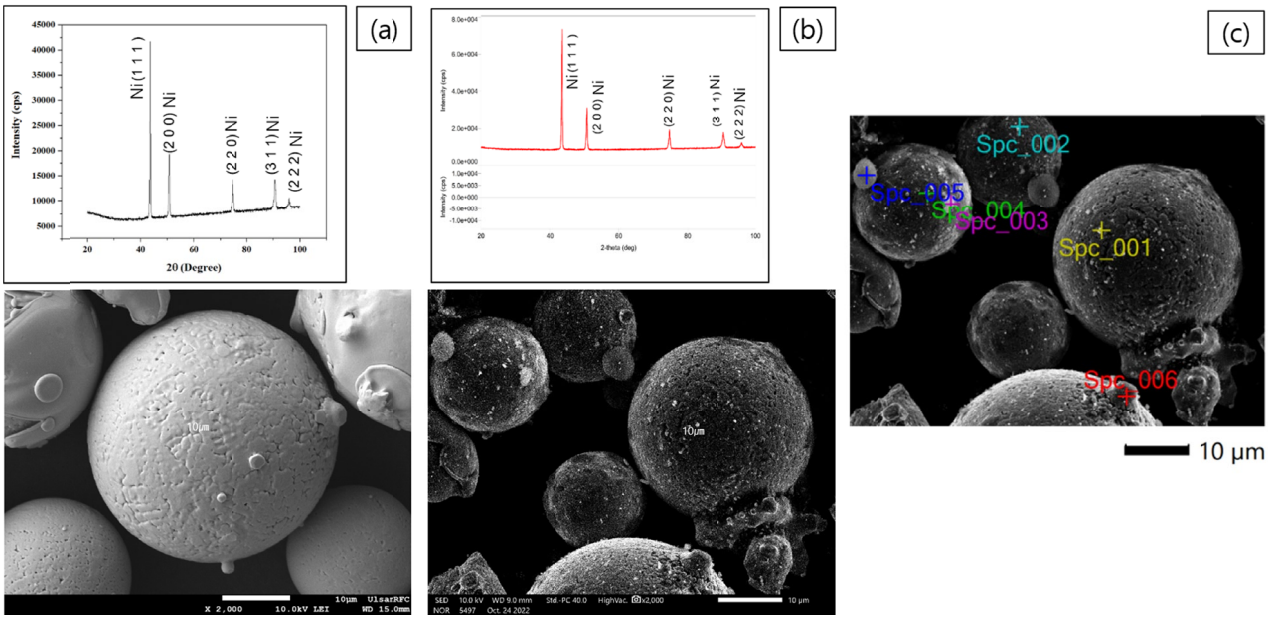

Fig. 1. SEM images and EDS elemental distribution of the powders before and after *ex-situ* mixing: (a) image of Inconel 738 powder, (b) image of Inconel 738 powder mixed with nano oxides, (c) EDS results of mixed powder

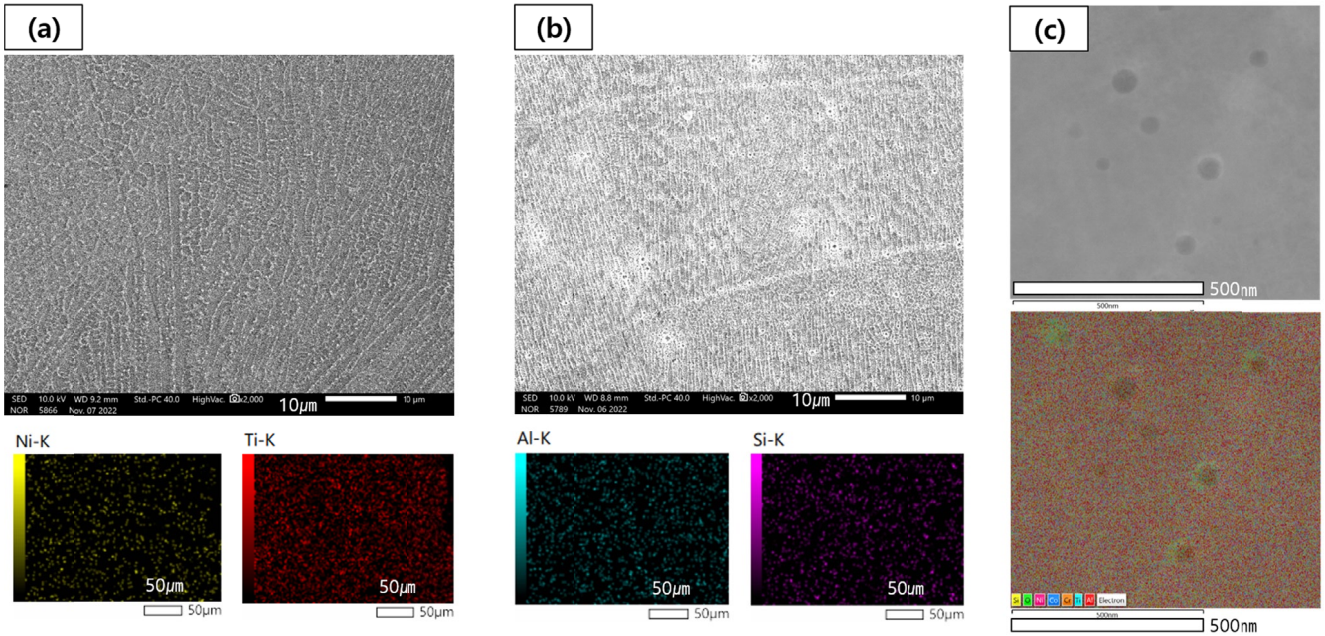

Fig. 2. SEM images and EDS elemental distribution of Inconel 738 specimen: (a) Inconel 738 PBF specimen, (b) Mixed Inconel 738 PBF specimen, (c) TEM and EDS mapping images of Mixed Inconel 738 PBF specimen

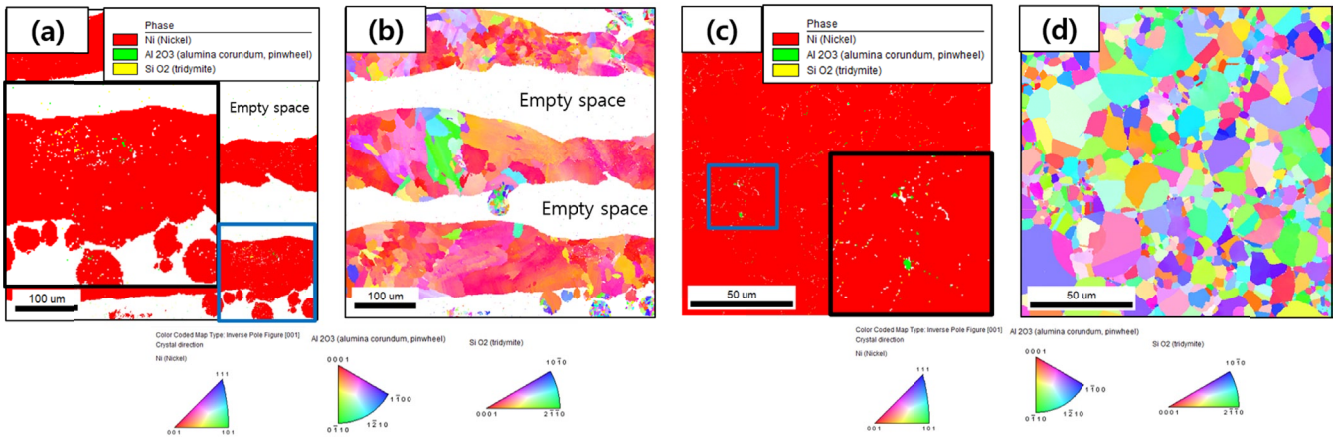

Fig. 3. EBSD analysis results of *ex-situ* L-PBF treated specimen and SPS specimen: (a) Phase map of mixed Inconel 738 specimen (b) IPF map of mixed Inconel 738 specimen. (c) Phase map of SPS Inconel 738 specimen, 1000°C. (d) IPF map of SPS Inconel 738 specimen, 1000°C.

Fig. 3. The crystal orientation of the specimens manufactured by L-PBF process were not uniform along the melting pool (laser direction). Ni phase having <001> direction was the main component and elongated with perpendicular of laser direction as shown in Fig. 3(b). Al and Si were detected uniformly along in the melting pool structure, as shown in the phase map (Fig. 3(a)). It means the nano-oxide particles, Al_2O_3 and SiO_2 was well dispersed in the melting pools. However, the SPS samples, we could see all direction of <001>, <101>, and <111> of Ni crystals as shown in Fig. 3(d). All grains had an equiaxed shape [14]. The nano-ceramic powders were not uniformly dispersed in the specimen (in Fig. 3(c). These nano-ceramic powders were segregated and distributed at the boundary of the 718 powder in the SPS samples.

4. Conclusions

In this study, we produced the mixed Inconel 738 powders with the SiO_2 and Al_2O_3 nanopowders using the *ex-situ* ball milling process, and subsequently, the L-PBF and SPS processes were studied. The ceramic nano-powders were found on the outer surface of the spherical Inconel 738 powders after mixing. The microstructure analysis showed that some irregular mixed dendrite microstructure and needle-shaped structure were formed in the L-PBF samples. Al and Si components were evenly distributed in the L-PBF specimen according to EDS mapping analysis. The oxide nanoparticles in the L-PBF were well dispersed in the melting pools by EBSD analysis. Ni phase having <001> direction was elongated with perpendicular of laser direction. However, in the SPS samples, all grains had exquiaxed shape and the nano-ceramic powders were not uniformly dispersed and

segregated at the boundaries. Thus, a uniform ODS dispersed microstructure using *ex-situ* ball milled powders can be obtained by the L-PBF process.

Acknowledgments

This work was supported by the Ministry of Trade, Industry & Energy (MOTIE, Korea Rep.) under Industrial Technology Innovation Program No. 20017647 "Development of oxide dispersion strengthened superalloy materials and manufacturing technology for hypersonic engines".
This results was supported by "Regional Innovation Strategy (RIS)" through the National Research Foundation of Korea (NRF) funded by the Ministry of Education (MOE) (2021RIS-003)

REFERENCES

[1] B. Dubiel, A. Czyrska-Filemonowicz, Inzynieria Materialowa **21**, 20-28 (2000).
[2] Ruifeng Xu, Zhaowen Geng, Yiyou Wu, Chao Chen, Mang Ni, Dan Li, Taomei Zhang, Hongtao Huang, Feng Liu, Ruidi Li, Kechao Zhou, Advanced Powder Materials **1**, 100056 (2022).
[3] Sanghoon Noh, Tae Kyu Kim, J. Korean Powder Metall. Inst. **28**, 5, 375-380 (2021).
[4] SeungHyeok Chung, Bin Lee, Soo Yeol Lee, Changwoo Do, Ho Jin Ryu, Journal of Materials Science & Technology **85**, 62-75 (2021).
[5] Raj Mohan et al., Hindawi Scanning 2022, (2022).
[6] J.B. Fogagnolo, M.H. Robert, J.M. Torralba, Materials Science and Engineering A **426**, 85-94 (2006).
[7] D.G. Morris, M.A. Morris, Materials Science and Engineering A **125**, 97-106 (1990).
[8] Ashwath Yegyan Kumar, Yun Bai, Anders Eklund, Christopher B. Williams, Additive Manufacturing **24**, 115-124 (2018).
[9] C. Selcuk, S. Bond, P. Woollin, Powder Metallurgy **53**, 7-11 (2010).
[10] M.M. Baloch, H.K.D.H. Bhadeshia, Materials Science and Technology **6**, 1236-1246 (1990).
[11] Sunil Kumar C. Pillai, Benoit Baron, Michael J. Pomeroy, Stuart Hampshire, Journal of the European Ceramic Society **24**, 3317-3326 (2004).
[12] Jose Alberto Muñiz-Lerma, Yuan Tian, Xianglong Wang, Raynald Gauvin, Mathieu Brochu, Progress in Additive Manufacturing **4**, 97-107 (2019).
[13] Sunil Kumar C. Pillai, Benoit Baron, Michael J. Pomeroy, Stuart Hampshire, Journal of the European Ceramic Society **24**, 3317-3326 (2004).
[14] Minghong Li, Lilin Wang, Haiou Yang, Shuya Zhang, Xin Lin, Weidong Huang, Materials Science and Engineering A **854**, (2022).